Fusion Engineering and Design 166 (2021) 112275

Contents lists available at ScienceDirect

Fusion Engineering and Design

journal homepage: www.elsevier.com/locate/fusengdes

Impact of materials technology on the breeding blanket design – Recent progress and case studies in materials technology

M. Rieth [a,*], M. Dürrschnabel [a], S. Bonk [a], G. Pintsuk [b], G. Aiello [c], J. Henry [d], Y. de Carlan [d], B.-E. Ghidersa [e], H. Neuberger [e], J. Rey [e], Christian Zeile [e], N. De Wispelaere [f], E. Simondon [a], J. Hoffmann [a]

[a] Karlsruhe Institute of Technology, Institute for Applied Materials, 76344, Eggenstein-Leopoldshafen, Germany
[b] Forschungszentrum Jülich GmbH, Institut für Energie- und Klimaforschung – Plasmaphysik, 52425, Jülich, Germany
[c] EUROfusion, PPPT, 85748, Garching, Germany
[d] Université Paris-Saclay, CEA, Service de Recherches Métallurgiques Appliquées, 91191, Gif-sur-Yvette, France
[e] Karlsruhe Institute of Technology, Institute for Neutron Physics and Reactor Technology, 76344, Eggenstein-Leopoldshafen, Germany
[f] OCAS NV, Pres. J.F. Kennedylaan 3, 9060, Zelzate, Belgium

ARTICLE INFO

Keywords:
Blanket first wall
Mockup
High heat flux test
Helium cooling loop
Materials technology
Engineering

ABSTRACT

A major part in the EUROfusion materials research program is dedicated to characterize and quantify nuclear fusion specific neutron damage in structural materials. While the majority of irradiation data gives a relatively clear view on the displacement damage, the effect of transmutation – i.e. especially hydrogen and helium production in steels – is not yet explored very well. However, few available results indicate that EUROFER-type steels will reach their operating limit as soon as the formation of helium bubbles reaches a critical amount or size. At that point, the material would fail due to embrittlement at the considered load.

This paper presents a strategy for the mitigation of the before-mentioned problem using the following facts:

- the neutron dose and related transmutation rate decreases quickly inside the first wall, that is, only a plasma-near area is extremely loaded
- nanostructured oxide dispersion strengthened (ODS) steels may have an enormous trapping effect on helium and hydrogen, which would suppress the formation of large helium bubbles
- compared to conventional steels, ODS steels show improved irradiation tensile ductility and creep strength

In summary, producing the plasma facing, highly neutron and heat loaded part of blankets by an ODS steel, while using EUROFER97 for everything else, would allow a higher heat flux as well as a longer operating period.

Consequently, we (1) developed and produced 14 % Cr ferritic ODS steel plates. (2) We fabricated a mockup with 5 cooling channels and a plated first wall of ODS steel, using the same production processes as for a real component. And finally, (3) we performed high heat flux tests in the HELOKA facility (Helium Loop Karlsruhe at KIT) applying short and up to 2 h long pulses, in which the operating temperature limit for EUROFER97 (i.e., 550 °C) was finally exceeded by 100 K. Thereafter, microstructure and defect analyses did not reveal defects or recognizable damage. Only a heat affected zone in the EUROFER/ODS steel interface could be detected. This demonstrates that the use of ODS steel could make a decisive difference in the future design and performance of breeding blankets.

* Corresponding author at: Karlsruhe Institute of Technology, Institute for Applied Materials, Hermann-von-Helmholtz-Platz 1, 76344, Eggenstein-Leopoldshafen, Germany.

E-mail addresses: michael.rieth@kit.edu (M. Rieth), michael.duerrschnabel@kit.edu (M. Dürrschnabel), simon.bonk@kit.edu (S. Bonk), g.pintsuk@fz-juelich.de (G. Pintsuk), Giacomo.Aiello@euro-fusion.org (G. Aiello), Jean.HENRY@cea.fr (J. Henry), Yann.DECARLAN@cea.fr (Y. de Carlan), bradut-eugen.ghidersa@kit.edu (B.-E. Ghidersa), heiko.neuberger@kit.edu (H. Neuberger), joerg.rey@kit.edu (J. Rey), christian.zeile@gmx.de (C. Zeile), nico.dewispelaere@ocas.technology (N. De Wispelaere), esther.simondon@kit.edu (E. Simondon), jan.hoffmann@ronalgroup.com (J. Hoffmann).

https://doi.org/10.1016/j.fusengdes.2021.112275
Received 30 November 2020; Received in revised form 16 January 2021; Accepted 21 January 2021
Available online 3 February 2021

1. Introduction

The European pre-conceptual design for a demonstration fusion reactor (DEMO) foresees a starter blanket (also referred to as driver blanket), which will be water or helium cooled, depending on the final choice of the breeding concept. In any case, the operating limit of the starter blanket is predefined by a neutron dose of 20 dpa. In a second operating stage, an advanced blanket will be tested with an extended lifetime corresponding to about 50 dpa (neutron dose). Based on today's material technology, this can only be achieved by increasing the operating temperature in the steel structures to 350 °C and above. Therefore, the coolant for the second (or advanced) blanket of the European DEMO reactor should/will be helium gas [1–4]. As with any other coolants, there are pros and cons connected with the helium gas cooling concept, like for example, balance of plant issues or a possible future shortage of the gas production, and others. In this context, other types of coolants that might also allow for a power plant operation at T > 350 °C (e.g., supercritical water [5], carbon dioxide [6], molten salt [7], liquid metals [8]) are discussed and explored as alternatives.

Regardless of the different breeding blanket concepts, the plasma-facing surface, and a layer of several millimeters – the so-called first wall – is the highest loaded part with regard to thermal as well as neutron load. Therefore, at least three main damage modes have to be taken into account: (1) thermal fatigue due to the pulsed plasma operation with some ten-thousand cycles, (2) neutron irradiation hardening and embrittlement as a consequence of displacement damage, and (3) material damage due to transmutation products, i.e., in steels this mainly leads to the formation of helium bubbles (but also hydrogen is produced).

A major part in the EUROfusion materials research program is dedicated to characterize and quantify nuclear fusion specific neutron damage in structural materials. While most irradiation data give a relatively clear view on the displacement damage, which is mainly responsible for the observed irradiation hardening, the effect of gas transmutation – i.e., especially helium production in ferritic/martensitic 9Cr-steels – has not been explored yet sufficiently. Nevertheless, available results indicate that EUROFER-type steels (the selected base and reference material within the European Fusion Project) will reach their operating limit when the formation of helium bubbles reaches a critical amount or size, which then leads to brittle fracturing [9–14]. Even though ferritic/martensitic steels show only a small tendency for swelling, this beneficial behavior might change significantly in the presence of helium, as observed in many studies on austenitic steels [15]. However, data on the effect of helium transmutation on void swelling in 9Cr steels are presently not available.

For future power fusion power plants, but also for the starter blanket (depending on the choice of the coolant) and in any case for advanced blankets of DEMO reactors, operating temperatures in the range of 450−550 °C (or higher) would be an effective measure to reduce irradiation hardening significantly (see, for example, [16–21]). In this case, the lifetime of helium-cooled breeding blankets would then be mainly determined by the thermo-mechanical load response (thermal fatigue) and by the accumulation and growth of helium bubbles.

In this paper, we present a possible strategy for the mitigation of the before-mentioned design limiting issues by making use of the following facts and assumptions:

- Neutron dose and related transmutation rates decrease significantly from the first wall towards the back plates, that is, only a plasma-near volume of the blanket is critically high loaded, which can be calculated by extensive quantitative simulations of neutron scattering events [14,22].
- Nanostructured oxide dispersion strengthened (ODS) steels can have an enormous trapping effect on helium and hydrogen, which then suppresses the formation of critically big helium bubbles [23]. In the case that helium is accelerating the void swelling in ferritic/martensitic steels (as mentioned above, this is not sufficiently explored, yet), the dispersoids in ODS steels would most probably reduce this effect, too, due their enormous sink strength for point defects. But this is a rather speculative assumption.
- Compared to conventional steels, ODS steels show better fatigue (and creep) resistance. That is, they can be operated at higher temperatures, which would substantially reduce irradiation hardening [24–30].

In summary, producing the plasma facing, highly neutron and heat loaded parts in blankets by an ODS steel (while using EUROFER steel for everything else), would allow a higher heat flux, a longer and safer operating period, and possibly more degrees of freedom in the design.

The extreme neutron loaded part in a blanket – which would have to be manufactured from an ODS steel – consists of a volume of about 0.2−0.3 m depth from the surface of the first wall (Fig. 1 gives an impression of the dimensions). This would require an amount of ODS steel in the order of several 100 tons, at least, and, presently, this would exceed the industrial production capability. Based on today's knowledge, this would probably be the most promising material and design strategy for a fusion power plant. For a DEMO reactor blanket, however, helium transmutation and related embrittlement does not play such an important role, since the starter blanket has a neutron dose limit of only 20 dpa. The critical helium limit might become relevant – if at all – in the advanced DEMO blanket (current design limit of 50 dpa) or it will be determined by material irradiation experiments in IFMIF/DONES. Therefore, one of several long-term goals is to develop appropriate industrial ODS production routes.

As a first step in this direction, another approach, which is not so ambitious but might still be interesting, can yield valuable information: If we focus just on the superior thermo-mechanical properties, an ODS steel layer on top of the blanket first wall could in principle allow higher coolant temperatures and longer component operating-times. For this, an ODS steel plating of 2−4 mm on top of a EUROFER based cooling structure (breeding blanket with cooling channels according to the current designs) would be necessary. That is, the demand of ODS steel for one advanced DEMO blanket (or blanket module) would range in the order of 40−100 kg while covering a complete DEMO blanket first wall would require about 20−40 tons. That is still beyond the current capability of steel industry, but if the production route of 100 kg ODS steel plates can be verified, an up-scaling to the several 10-ton ranges seems to be feasible.

With a focus on the second approach, the first verification of the before-mentioned strategy required about 7 years – starting with the idea and ending after the final destructive analyses – during which we followed (most often in parallel) three main lines of research,

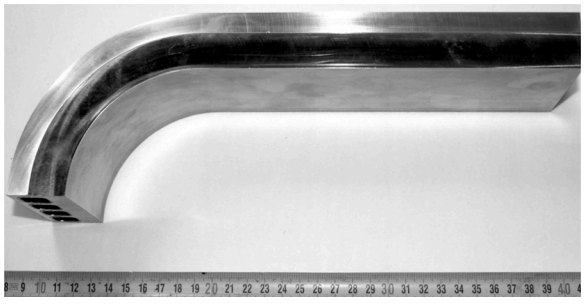

Fig. 1. Cut through a first wall mock-up with four internal cooling channels (the ruler scale is in centimeters). The plasma-facing surface is on top with the cooling channels located 3 mm beneath. This mockup was fabricated by diffusion welding of two grooved and bended plates with inserted cooling pipes [31]. The depth of 0.3 m corresponds approximately to the real blanket boxes in the current pre-conceptual design. On the left-hand side, a side plate would be attached. and the top and bottom would be closed by caps. The surface of a real blanket box would be amount to roughly 2 m^2.

development, and investigation: (1) production of thin ODS steel plates on a larger scale (i.e., in the order of 100 kg), (2) design and fabrication of a testable first wall (of a DEMO breeding blanket) mockup, and (3) cyclic high heat flux loading in a helium cooling loop. These activities are outlined in the following chapter. Thereafter, we present the outcomes of high heat flux tests, which are followed by a detailed analysis and discussion of the results on microstructural examinations of the mockup after the tests. In the final sections we conclude the investigative findings.

2. Experimental setup and related R&D

To our knowledge, plate fabrication of low-activating ferritic ODS steel has never been developed for the specifications given above, that is, in the 100 kg range and for a thickness of 2−4 mm. Therefore, the main focus was laid on the rolling procedure after the material selection and specification was performed.

The design and fabrication of a testable first wall mockup with an ODS steel plating could be performed, based on a comprising expertise that has been accumulated over the last decade within the European Fusion Projects EFDA and EUROfusion, in which already many basic material-technological experiments and studies were accomplished. Nevertheless, the mockup we discuss and report in this paper is a first-of-its-kind, worldwide.

For both, plate rolling and mockup fabrication, we placed the emphasis on industrially available or technologically scalable processes.

The third novelty is the cyclic high heat flux test in a helium cooling loop under such extreme conditions, in which the surface temperature of a first wall mockup could be intentionally increased above the common 550 °C operating limit of the nuclear fusion steel EUROFER97.

2.1. Material selection, specification, and production

The manufacturing processes and the most important properties of a broad range of low-activating ODS steels are well-known and have been widely explored, studied, and discussed (an overview is given in [32–35] and references therein). Out of this knowledgebase, a ferritic ODS steel with the chemical composition 14Cr-1W-0.2Ti-0.2Y_2O_3 (numbers in weight %) was chosen as the plating material for this project. The reason for the lower as usual Ti and Y_2O_3 concentrations is to lower the recrystallization temperature. A higher density of Ti-Y-oxide particles could cause problems during plate manufacturing (e.g., abnormal grain-growth during recrystallization). However, with these specifications the final product was expected to still have very good high-temperature properties, which would meet the requirements for the chosen application, although the creep performance would be somewhat lower than that of a 14Cr alloy with higher Ti and Y_2O_3 concentrations.

However, the objective of this task is the manufacturing of 4 mm, 3 mm, and 2 mm thick plates in a quantity of about 100 kg as a demonstration of a feasible industrial production route. For this, several companies were involved at the different stages of the industrial processes. Nanoval was the powder-producer, Plansee was responsible for mechanical alloying, Aubert-Duval was charged with powder vacuum canning, Bodycote was designated for hot isostatic pressing, and OCAS oversaw the hot-cross rolling optimization of the plates and the final cold rolling. The coordination, quality assurance, and characterization was performed by CEA.

The production of the powder has involved atomization with argon using the Nanoval Process to a powder with d50 (mean diameter) about 30 μm, while the constraint on the 90 % of the procurement is to have dimensions lower than 120 μm.

Nanoval produced a total of 164 kg of powder by atomization with argon gas. The powder particles showed a mean diameter d50 of about 30 μm with a constraint on 90 % of the procurement of particle dimensions lower than 120 μm. After production, the powder was shipped in containers (each with 10−14 kg) under protective argon atmosphere to CEA Saclay. The particle size distribution, measured by Nanoval using a Laser diffraction sensor (HELOS instrument), was in good agreement with the specifications. Chemical analysis revealed that the titanium content of 0.16 wt.%) is slightly lower compared to the expected value of 0.2 wt %, but it was considered that this powder is well suitable for the mechanical alloying. So, 140 kg of the Nanoval powder was sent to Plansee for the mechanical alloying (MA). Plansee added 0.2 +/- 0.05 wt.% Y_2O_3 powder and performed MA in an industrial facility under pure hydrogen. Then the milled powder was sieved, which left 109 kg of powder with a particle size lower than 100 μm. This corresponds to an output of about 75 % of the total amount of material. The final chemical composition is compiled in Table 1. Finally, the milled and sieved powder was filled in plastic containers under air and sent back to CEA.

The next step – powder consolidation – was conducted by the companies Aubert et Duval and Bodycote. For that, two containers of 316 steel were fabricated, filled with the powder, degassed, and sealed (Aubert et Duval). Then, the containers were hot iso-statically pressed by Bodycote at 1160 °C for 3 h at 102 MPa. Finally, two blocks were machined to the size 125 mm x 125 mm x 125 mm (each of 15 kg). These were the semi-finished products for the rolling studies at OCAS, which are outlined in the following.

To avoid decarburization, the first block was packed in a stainless-steel strip before being rolled from 125 mm to 63 mm with a reduction of 10 % per pass. The initial rolling temperature was 1100 °C. In the subsequent hot-rolling passes, the temperatures were not acquired. However, a conservative estimate leads to a temperature drop lower than about 100−200 K. Due to the low thickness to length ratio, the ends of the ODS sheet take a V shape in rolling direction, which often promotes the initiation of cracks. Therefore, after reaching a thickness of 63 mm, we continued with cross-rolling. For this, the plate was heated to 1100 °C again to recover ductility, and then the sheet was cross-rolled to a thickness of 5 mm.

During cross rolling, a formation of small cracks on the edges of the sheets could be observed. Fortunately, the length of these small cracks remained stable, and therefore, the ODS steel could be further hot-rolled to the specified thickness.

Cold rolling (i.e., without pre- or active heating) hard materials such as ODS steels is a delicate and non-trivial matter. Therefore, different studies were conducted on instrumented rolling mills, which display and record displacements and forces during processing the plates. Fig. 2 shows an exemplary diagram for such a rolling experiment. It shows the rolling forces, the thickness of the sheet, and the gap between the rolling cylinder. During the initial cold-rolling phase, the cylinder gap is wider than the thickness of the sheet. As the process progresses, the cylinders come closer and cold deformation takes place. In this phase, the sheet thickness follows the cylinder gap. After 15 rolling steps, reaching a thickness of about 2.6 mm, the sheet is almost no longer deformed and the mismatch between cylinder gap and sheet thickness is reaching about 0.3 mm. At this point, a heat treatment was performed (at 1100 °C for 5 min) in order to reduce the hardness and to prevent cracking the material. Then, the cold-rolling process was continued. As can be seen in Fig. 2 (see the part encircled by a dashed line), the heat treatment has significantly increased the ductility of the plate and it could be cold-rolled to the final thickness of 2 mm in the second rolling sequence (step no. 16-21). Of course, recrystallization should not take place during the recovery treatment. This has been verified in a separate study where hardness was measured after different iso-chronal annealing experiments.

With this manufacturing route, two sheets of 1200 mm x 230 mm x 2 mm were produced (Fig. 3). For the second block, in principle the same plate production route was set up. But to avoid the V-shape deformation at the rolling ends during hot-rolling as well as for a reduction of cracks at the edges of the sheet, the ODS steel block was embedded in a bigger cylindrical steel block. After hot-rolling, the surrounding steel was removed and cross-rolling was performed on the ODS steel block alone.

Table 1
Chemical Analysis (in weight % and weight ppm) of the MA powder, according to Plansee.

	Cr	C	Mn	W	N	O	Y	Ti	Ni	H
milled powder	135 %	164 ppm	917 ppm	0.99 %	78 ppm	0.117 %	0.146 %	0.16 %	559 ppm	57 ppm

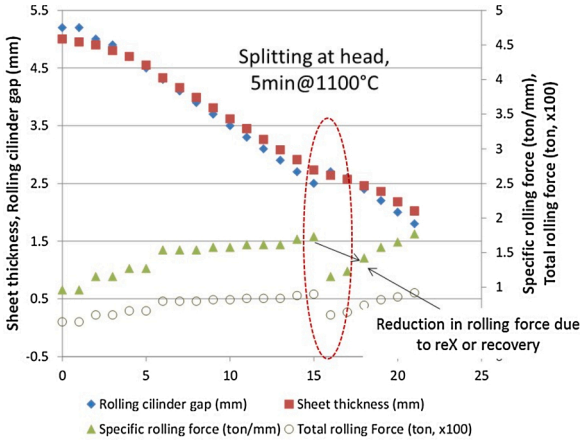

Fig. 2. Suitable parameters for the ODS steel plates were determined by cold-rolling experiments using small strips and by evaluation of the readout of the instrumented rolling mills at OCAS. In this example, rolling was stopped after the 15th step to avoid cracking the plate. Then the plate was recovered and/or recrystallized for 5 min at 1100 °C, which resulted in a significantly lower rolling force in the following few steps (encircled in a dashed line in the diagram). More details are given in the text.

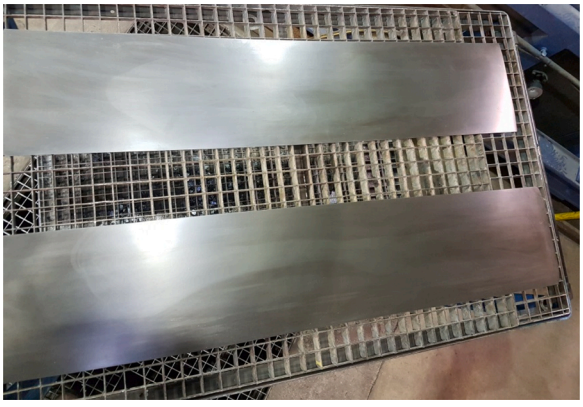

Fig. 3. The final 2 mm thick ODS steel plates with a size of 1200 mm x 230 mm, which were produced from a consolidated powder block of 125 mm x 125 mm x 125 mm by hot and cold-rolling.

By this technique, 4 additional plates of 3 mm (1000 mm x 100 mm) and 2 mm (1300 mm x 100 mm) thickness could be produced.

2.2. Mockup design and fabrication

The objective of the mockup design was to get a down-sized representative model of the first wall of a DEMO reactor that can be installed in the Helium Loop Karlsruhe (HeLoKa) for high heat flux tests. There are four DEMO blanket concepts: two with water and 2 helium as a coolant. In principle, the ODS plated first wall configuration could yield advantages, e.g., in terms of longer life-times, for all concepts. But the water temperature is limited in a sub-critical operation (super-critical water cooling has not been taken seriously into account for a DEMO reactor). Therefore, the benefit of ODS steel plating might be even higher for the helium cooled concepts by possibly enabling increased coolant temperatures. From a fabrication point of view (with a focus on the ODS steel plating), there are no big differences between the blanket concepts, either. Thus, we decided to use the Helium Cooled Pebble Bed (HCPB) breeding blanket concept as a reference for the mockup, its design, and fabrication. A detailed description can be found, for example, in [36–38] and references therein.

For the mockup fabrication, we followed a sequence of fabrication steps, which are in principle also applicable to the manufacturing of real-size breeding blankets: (1) fabrication, machining, and preparation of ODS and EUROFER97 steel plates, (2) encapsulation and evacuation of both plates followed by vacuum-tight sealing, (3) diffusion bonding of the plates in a hot isostatic press (HIP), and (4) machining the cooling channels. As reviewed in [39,40], there are several possible fabrication concepts and sequences for the blankets. Some of these would require bending the plates into U-shape (see Fig. 4) after step (1), (3), or (4). For the mockup we neglected bending, that is, the mockup represents only the flat part of a first wall. In the following, the 4 fabrication steps are outlined.

Step (1): We determined a mockup size (plane first wall with internal cooling channels) of about 160 mm x 200 mm x 24 mm as suitable for the installation into the helium cooling loop. Therefore, we machined a massive base plate of EUROFER97/2 (thickness 25 mm, heat no. 993,991) and a matching ODS plate (thickness about 5 mm) by sawing and milling. Both plates were slightly oversized to allow a final precise finish after diffusion bonding.

In the previous section we outlined the industrial upscaling of the ODS plate production processes and showed how bigger quantities could be produced. But the plates from this R&D work were not available for the mockup fabrication since their production took place much later. So, we produced a lab-scale batch of ODS steel that was tailored to the mockup fabrication. For that, pre-alloyed powder (5 kg) was mechanically alloyed together with yttria powder in hydrogen atmosphere in an industrial Attritor ball mill at Zoz GmbH in Germany. The as-milled powder with a chemical composition of Fe-13Cr-1.1W-0.3Ti-0.3Y_2O_3

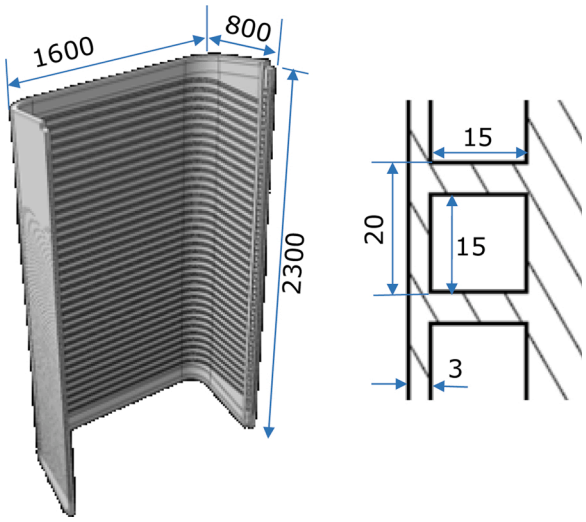

Fig. 4. (left) Typical layout for the U-shaped first wall of a HCPB blanket with the internal cooling channels indicated. (right) Cross-section of the first wall with exemplary dimensions of the cooling channels. Notes: the distance of the channels from the surface (plasma side) is only 3 mm while the length/diameter ratio is more than 200).

was packed in Argon and sent to KIT for further processing in an Argon-filled glove-box to protect the powder from oxidation in air. Here, it was sieved and the fraction between 45 μm and 90 μm powder particle diameter was taken out. From this, 2.6 kg were filled in a cylindrical 316L stainless steel capsule (diameter of 80 mm, height of 170 mm). After degassing at 400 °C in vacuum, the capsule was sealed and then hot-isostatic pressed at 1100 °C with a pressure of 100 MPa for 2 h holding time. After taking off the top and bottom of the capsule, it was sent to OCAS in Belgium for tempering and hot-cross-rolling at 1050 °C. The rolling scheme with the reduction for each step is given in Table 2. After pass number 5, the capsule was reheated for 10 min. When the rolling temperature of 1050 °C was reached again, the capsule was turned for 90 °C and rolled in this direction. The final shape of the plate after pass 11 is shown in Fig. 5.

The stainless steel capsule wall was left on for the whole rolling process. This gives the advantage of reducing the thermal shock to the material, preventing hot cracking and oxidation of the ODS material due to the high rolling temperature.

An electron back-scatter diffraction (EBSD) scan of the plate in the transvers view is shown in Fig. 6. The map is calculated along the rolling direction (RD) and displays a strong <110> orientation (green color in Fig. 6) of the grains, which also have a high aspect ratio with an elongation along the RD. The grain size is in a typical range for ferritic ODS alloys. Looking more into detail reveals a pronounced sub-structure within the larger grains, in which sometimes high orientation gradients occur. This has also been reported for other ferritic ODS alloys produced in a similar way.

To complete the microstructural investigations, the orientation distribution function (ODF) was calculated to show the crystallographic texture. A section through the ODF (phi2 = 45°) is given in Fig. 7. The components of both, the alpha- and gamma-fiber texture can be observed. The overall intensities with a maximum value of nearly 20 times random are rather high, which corresponds to a pronounced rolling texture.

Finally, the ODS steel plate surfaces were milled down about one millimeter to remove the leftovers of the stainless-steel capsule. This proved to be challenging due to residual stresses stored in the material after cross rolling. Even a tempering treatment at 800 °C for 2 h did not remove the stresses significantly. For this reason, holes were drilled into the border area to flatten the plate onto the specimen holder during milling. Nevertheless, vibrations during milling caused grooves and an overall rougher surface than usual after milling (see Fig. 8). Since such imperfections might have to be tolerated in an industrial production, we continued the mockup fabrication and took this as a robustness test. The bonding surface of the EUROFER plate was also milled over (by about 0.1 mm) to remove the oxide layer and Ito ensure a proper diffusion weld process.

Step (2): Instead of the usual encapsulation, we applied the following procedure: The ODS and EUROFER97/2 steel plate were fixed together in an electron beam (EB) welding facility. Then, a circumferential weld seam with a penetration depth of about 3 mm was prepared. Since the EB weld facility works in vacuum, both plates were encapsulated, evacuated, and sealed in one step (see also [31,41,42]).

Step (3): Diffusion bonding of the ODS plate with the EUROFER97/2 steel was be accomplished at Bodycote, Germany, by hot isostatic pressing (HIP) in an industrial press with temperature and pressure control. Based on previous studies, the joining was carried out for about 2 h at 1100 °C with a pressure of 100 MPa.

Step (4): After joining, the block was milled to the final outer dimensions of 208 mm x 160 mm x 23.5 mm, reducing the thickness of the ODS steel plate to 3 mm in the process. Then the block was sent to KRÜGER ERODIERTECHNIK for electro-discharge wire-cutting the

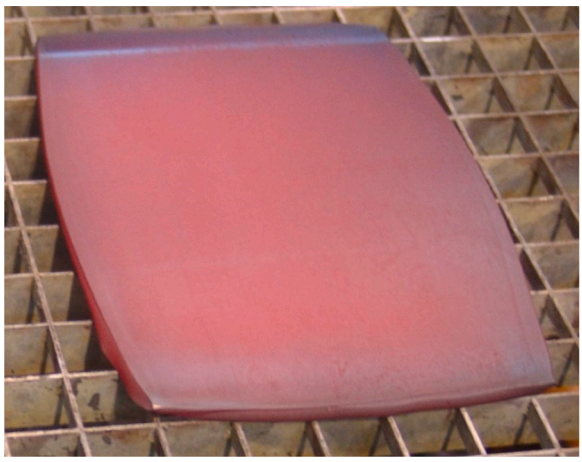

Fig. 5. Fe-13Cr-1.1W-0.3Ti-0.3Y_2O_3 ODS steel plate after cross rolling at 1050 °C (4 passes longitudinal, 7 passes transversal).

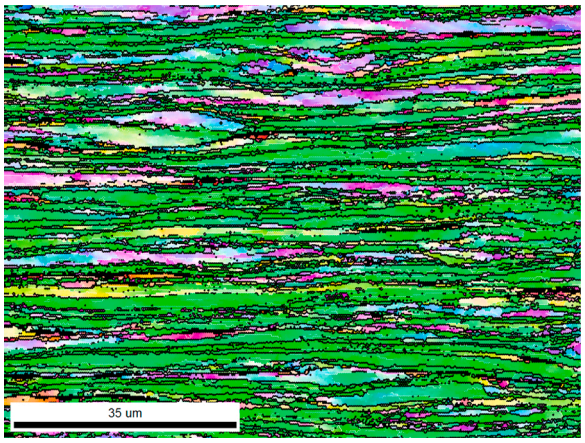

Fig. 6. Microstructure of the ODS steel plate in as-rolled condition (EBSD scan, transverse view along rolling direction, step size 300 nm, green colored areas correspond to <110> orientation).

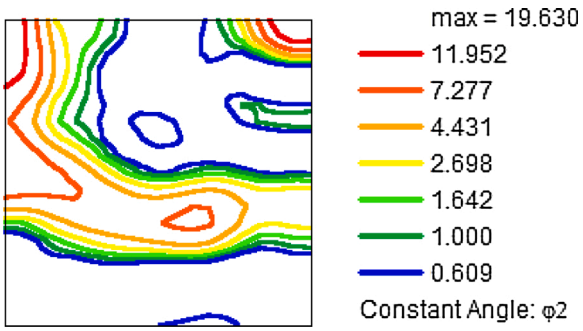

Fig. 7. Phi2 = 45° section through the ODF.

Table 2
Rolling scheme for 11 passes – reduction and plate thickness (including capsule material at the surfaces) after each rolling pass.

Pass No.	initial	1	2	3	4	5	6	7	8	9	10	11
Reduction (%)	–	16	20	22	20	20	15	20	20	20	20	20
Thickness (mm)	65	54.6	43.7	34.1	27.3	21.8	18.5	14.8	11.9	9.5	7.6	6.1

Fig. 8. ODS steel plate after removing the capsule residues from the top and bottom surface. The arrow indicates an area of milling grooves that occurred due to vibrations during milling.

cooling channels according to the drawing in Fig. 9 (more details are given in [36–38]). This fabrication step can already be performed on real-size components up to 3 m length. We reduced the cooling channel cross-section to 10 mm x 15 mm (with 2 mm radii at the corners) according to an update in the DEMO blanket design. We increased the distance from the surface to the channel to 3.5 mm for the 2 left and 2 right channels.

Now it is important to highlight the following design issue: The height of the middle channel was intentionally increased to 11 mm, so that the upper part runs into the ODS steel plate. This means that the cross-section of the middle channel crosses the diffusion weld area (Fig. 9). Therefore, the middle channel includes two weld seams along both upper corners. Since the corners are the highest stressed regions in the mockup plate (due to the stress concentration along the 2 mm radii), we have produced artificial crack initiators, which we expected to develop or even fracture during the high heat flux tests. weakened the design significantly.

In summary, the mockup fabrication was performed using solely industrial based or commercially established processes, which could also be applied to the production of the real components – the breeding blankets. The fabrication included two weak points that would allow to assess the robustness of the design in terms of (1) small imperfections in machining and handling a 2 m^2 size surface of a massive component in the several tons range within an industrial environment and (2) possible crack initiation domains due to fabrication, material, operational, or processing shortcomings. The first one refers to milling grooves in the surface of the ODS steel plate that have not been removed before diffusion bonding, while possible crack initiation lines were included intentionally by design. Such a bold defect would most probably not occur in the real production process. In this case, however, the intention was to accelerate the time to failure during the high heat flux test, and, therefore, to determine the robustness of the outlined fabrication approach.

2.3. Instrumentation, installation, Helium Loop Karlsruhe

In the frame of the EUROfusion work package breeding blanket (WPBB), subcomponent tests in helium facilities were foreseen. In this connection, we took the opportunity to modify and extend an already planned test campaign. In the following, we report the preparation of the experimental testing of our first wall mock-up in the Helium Loop Karlsruhe (HELOKA) that is described in detail, for example, in [43–46]. The work includes the following activities:

- Engineering design of the experimental setup
- Design of the helium inlet/outlet manifolds, or in other words, distributors
- Design of the fixation for the mock-ups
- Design of the piping layout (not reported here)
- Manufacturing of the experimental setup

2.3.1. Engineering design of the experimental setup

We designed the experimental setup for a parallel installation of two mockups next to each other in the HELOKA vacuum tank, that is, one test position for our mockup and another for a FW mock-up with Functional-Grading W/EUROFER coating, which we will disregard. This reduces the time required for the experimental campaign as the installation of the mockups and the piping between the mock-ups and the HELOKA manifolds as well as between the vacuum tank and the HELOKA loop can be done in one-step.

Both mock-ups have five cooling channels with a rectangular cross section of 15 mm x 10 mm, that are supposed to be connected to the helium loop. Due to the similarity of the channel geometry of the two mock-ups, a common design the helium distributor, which connects one inlet or outlet pipe to the cooling channels, was preferred and thus developed.

2.3.2. Design of helium distributors

The goal of the design of the helium distributor is to allow a homogenous mass flow distribution in the five channels. For this reason, several distributor designs have been developed considering a total mass flow rate of 40 g/s in each channel (i.e., 200 g/s in total), an inlet temperature of 300 °C and an inlet pressure of 8 MPa. The mass flow distributions of the different designs have been evaluated based on CFD analyses. The finally selected design, which also allows for a relatively easy manufacturing, is shown in Fig. 10. The corresponding velocity profile in the distributors and the ODS mock-up can be seen in Fig. 11. The mass flow rates in the helium channels of the ODS mock-up are listed in Table 3. Here, the computed maximum deviation of 4% relative to the nominal mass flow rate is fully acceptable since it will have a negligible effect on the temperature distribution on the mock-up during the experiment. Furthermore, the total pressure-drop in the distributors and in the mockup have been calculated to be 0.05 MPa only.

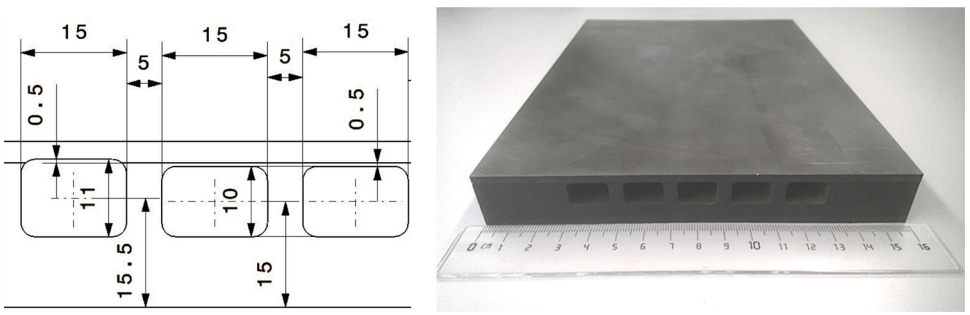

Fig. 9. (left) Drawing of the cooling channels as fabricated by electro-discharge machining (EDM, wire cutting). The channel in the middle (the left one in the drawing) is higher by one millimeter compared to the other four. That is, this channel cross-section exceeds the baseplate of EUROFER97/2 and includes the diffusion weld-lines along both upper corners. Therefore, we have intentionally placed the potentially weakest points (the weld seam) in the area of highest stress (this is due to stress concentration along the 2 mm radii of the corners). (right) The joined mockup block after EDM of the cooling channels.

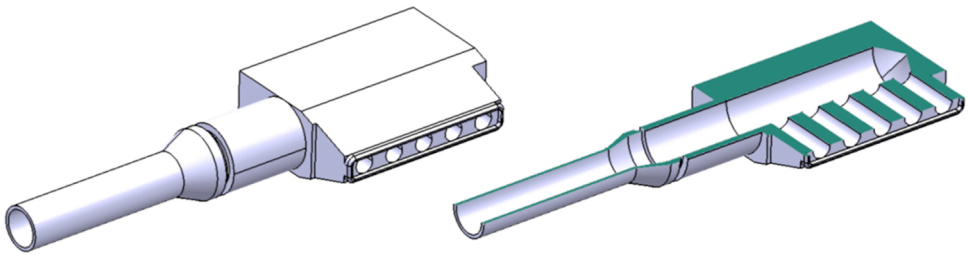

Fig. 10. Helium distributor (left) and section view (right).

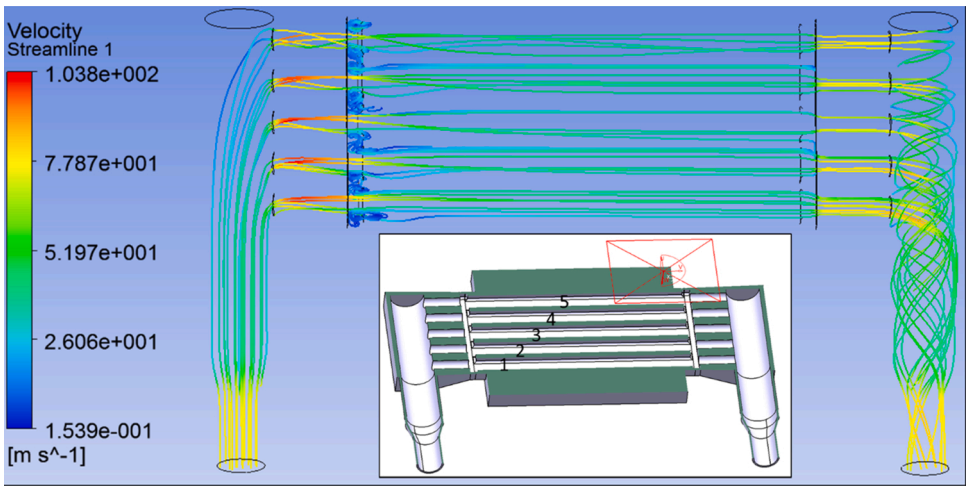

Fig. 11. A CFD simulation for the velocity profile of the helium gas in the cooling channels of the mockup.

Table 3
Mass flow rate distribution in the mockup cooling channels according to the CFD analyses.

Channel	Mass flow in g/s	Deviation from nominal
1	38.4	−4 %
2	39.5	−1 %
3	41.4	+3.5 %
4	40.2	+0.5 %
5	40.4	+1 %

2.3.3. *Design of fixation*

The fixation for the two mock-ups is designed in such a way that it allows free thermal expansion of the structure while restricting the overall movement of the mock-ups. As can be seen in Fig. 12, water-cooled plates are mounted on the support beam in the HELOKA vacuum tank. A holding plate that lies on the water-cooled plates is bolted to two U-100 profiles by means of flanges on each side. Two M-12 threaded rods extending from holding plates to the other side of beam fixes U-100 profiles with the beam. Each mockup is connected to the holding plate by four screws in slotted holes to accommodate the

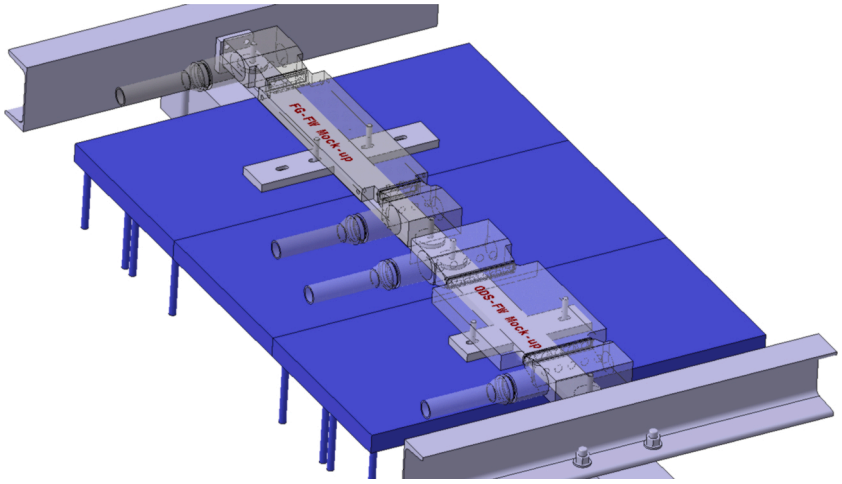

Fig. 12. Experimental setup for mounting two mockups on the support beam. Our mockup is labeled “ODS-FW Mock-up”.

thermal expansion. Ceramic discs provide a thermal insulation between mock-ups and holding plate. To avoid heating outside a predefined specific surface area of the mockup, in particular the weld joint between the distribution manifolds and the FW segment, cooling plates were put into place for a protection of these mockup areas.

2.3.4. Manufacturing of helium distributors, reducers, and assembly to the mockup

The final mockup consists of five parts: the mockup plate with 5 cooling channels, 2 helium distributors, and 2 reducers. Before these parts can be joined, the first wall plate had to be modified by milling connectors on both ends that fit to the distributors (Fig. 13: Mock-up plate after milling the connectors to both ends (side view).). Then, the distributors and reducers were machined from P92 steel (a conventional 9Cr-2W-Mo steel, type 1.4901) and all parts were tungsten-inert-gas (TIG) welded. The layout and weld seams are depicted in Fig. 14.

Welding was performed in two steps: In the first step, the reducer and helium distributors were assembled (TIG welds 2) followed by a post-welding heat treatment (PWHT) of these parts. After the final assembly of all parts (TIG welds 1 + TIG welds 2), a second PWHT was applied to the full assembly. The PWHT followed the EUROFER97 standard heat treatment of 980 °C/1 h + quenching +750 °C/2 h to optimize the component for creep strength and toughness. The second PWHT was performed on the whole mockup. Finally, the welds were examined by liquid penetration as well as by ultra-sonic testing. Both revealed no cracks or leaks.

2.3.5. Pressure test of the mock-up

Before the installation of the mock-up in HELOKA, a pressure test according to EN 13455−5:2014 with helium gas was completed. The test pressure was calculated based on the material properties of EUROFER97/2 as specified in the code "RCC-MRx Demande de modification/Modification request DMRx number: 10–115 A3.Gen et A3.19AS Eurofer", dated: 28.06.2010. The test pressure P_t is defined in EN 13455−5:2014 as follows:

$$P_t = 1.25\ P_d\ \frac{f_s}{f_{T_d}} = 1.25\ P_d\ \frac{R_{p0.2\ (20\,^\circ C)}}{R_{p0.2\ (600\,^\circ C)}} = 1.25\ \times 10\ MPa\ \times\ \frac{546\ MPa}{286\ MPa}$$
$$= 23,9\ MPa$$

with design pressure P_d and the ratio between strength properties of EUROFER97 at test temperature and operating temperature $f_s\ /\ f_{T_d}$. The holding time of the pressure test was 30 min. The mockup passed the test without any problems and, therefore, was cleared for the installation and operation in the high heat flux test facility, which is shown in Fig. 15.

2.3.6. Testing instrumentation

The facility and mockup had to be instrumented to measure and record the following parameters during the experiment for relevant points in time:

- Temperature on the mock-up surface by infra-red (IR) camera
- Temperature helium mock-up inlet/outlet with thermocouples
- Total mass flow through mock-up with two orifice mass flow meters
- Absolute pressure helium at mock-up inlet

For the temperature measurement thermocouples (TC) type K class 1 with 3 mm outer diameter were installed. The sensors are placed directly

Fig. 13. Mock-up plate after milling the connectors to both ends (side view).

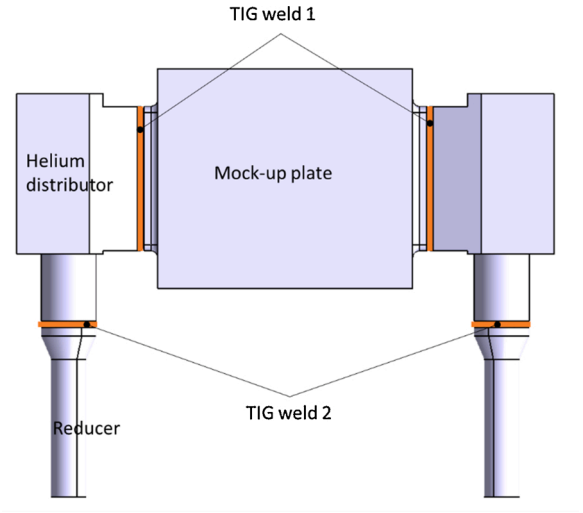

Fig. 14. Fabrication of the ODS mock-up.

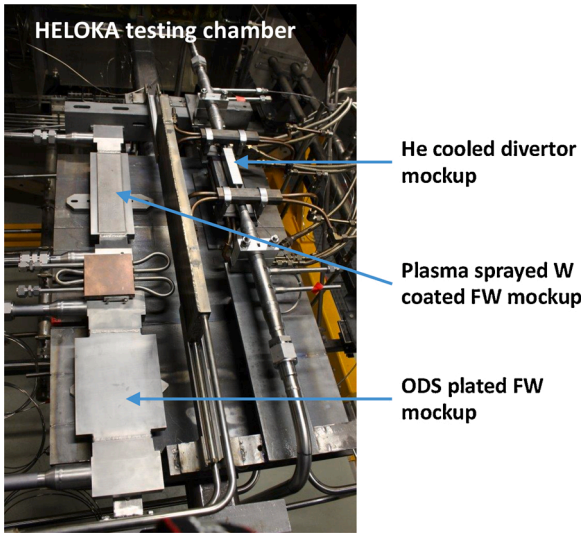

Fig. 15. View into the testing chamber of the HELOKA facility. For the present test campaign, beside our ODS steel plated first wall mockup, there was another first wall and a divertor mockup installed on the same test frame.

in the helium stream, upstream from the inlet nozzle and downstream from the outlet nozzle, respectively. The TCs were connected directly to National Instruments 9214 modules with its special terminal blocks. The mock-up surface temperature was measured with a thermal imaging infrared (IR) camera (FLIR X6580sc). The readings of the camera were calibrated at the beginning of each experimental session by adjusting the camera parameters while maintaining the mock-up at constant temperature (300 °C). This is done by heating-up the mock-up only by using the coolant flow and controlling the helium temperature until a steady state is achieved. The camera measurement accuracy is ±1 %. Past experiments have shown that, for EUROFER97 or similar materials, the changes in surface emissivity with temperature have a marginal impact on the measurements within the expected temperature range (300 °C–600 °C).

For the flow measurements orifice flow meters have been chosen. The sensor transducers, Siemens Sitrans P DSIII / P410, were set and calibrated in the factory to provide directly the volumetric flow rate. The mass flow rate was calculated during the data acquisition process by the National Instruments data acquisition and control system cRIO-9025. The helium density needed in the calculation of the mass flow is

calculated using a temperature and pressure measurement downstream of the orifice according to the equation 2−1 from [47]. The temperature sensor used for these measurements is of the same type as the one used for measuring the inlet/outlet helium temperatures, while the pressure sensors are of type DMP 320, from BD Sensors GmbH, with an accuracy below 100 mbar.

3. Results and discussion

3.1. High heat flux fatigue tests

The European DEMO operating scenario for the starter blankets includes cycle numbers in the order of 10000. Since that would have exceeded our available time contingent of the facility, the emphasis of this first experiment was rather placed on probing higher surface temperatures (i.e., 600 °C or even higher) than performing realistic cycle numbers.

The test matrix has been defined based on finite element simulations and thermo-mechanical analyses of various loading configurations and coolant inlet temperatures that would guarantee the structural integrity of the mock-up during the test cycles at high surface temperatures. The stresses in the mock-up have been evaluated according to the RCC-MRx code. As a conservative approach, the material limits of EUROFER97/2 have been applied to the analysis of the whole mock-up plate.

The simulations showed that the safest configuration (regarding the weld seams between the plate and manifolds) is obtained when the heat load is limited to a zone of 100 mm × 100 mm as shown in Fig. 16. This area spans over all 5 cooling channels in transverse direction to the channel axis, but amounts to only about half of the channel length. In this way, the maximum stress levels occur in the central zone of the mock-up and not in the vicinity of the weld junctions, as would be the case, if the full channel length was loaded. This loading configuration allows a maximum surface temperature of 600 °C at 0.8 MW/m^2 heat flux while keeping the stress level just below the material limits. The complete set of testing parameters for this reference scenario is compiled in Table 4 and the resulting simulated surface temperature distribution is shown in Fig. 16.

The stresses on the mock-up during the reference scenario have been evaluated according to the RCC-MRx code. As a conservative approach, the material limits of EUROFER97/2 have been considered for the evaluation of the stresses for the whole mock-up plate. The evaluation has shown that the design fulfills the rules given by the design code for the reference scenario and exploits at the same time the material limits as much as possible.

Table 4
Test parameters for the reference scenario that guarantees a safe operation according to the simulation.

Maximum heat flux	0.8 MW/m^2
Total mass flow	0.2 kg/s
Helium inlet temperature	300 °C
Helium pressure	8 MPa

The following parameters were measured during the experiment and recorded for relevant points in time:

- Temperature on the mock-up surface by IR-camera
- Temperature helium mock-up inlet
- Temperature helium mock-up outlet
- Total mass flow through mock-up
- Pressure helium at mock-up inlet
- Pressure helium at mock-up outlet

After the installation of the mock-up in HELOKA, several initial tests were performed to check the entire setup and to calibrate the instrumentation and the electron beam gun. During these initial tests, the power of the electron beam was gradually increased to finally reach a steady-state condition with a surface temperature on the mock-up plate close to 600 °C. After the installation of the mock-up in HELOKA, several initial tests were performed to check the entire setup and to calibrate the instrumentation and the electron beam gun. During these initial tests, the power of the electron beam was gradually increased to finally reach a steady-state condition with a surface temperature on the mock-up plate close to 600 °C. Having the outlet temperature sensor installed downstream from the mock-up, the initial testing phase was also used to determine the shortest loading time that allows for a calorimetric evaluation of the heat load. Thus, the tests showed that using a loading time of 2 min the outlet temperature measurement reaches a stationary level.

After these initial tests, the mockup was loaded according to the defined goals, that is, high heat flux tests were carried out by operating the test facility in the reference scenario with the electron beam

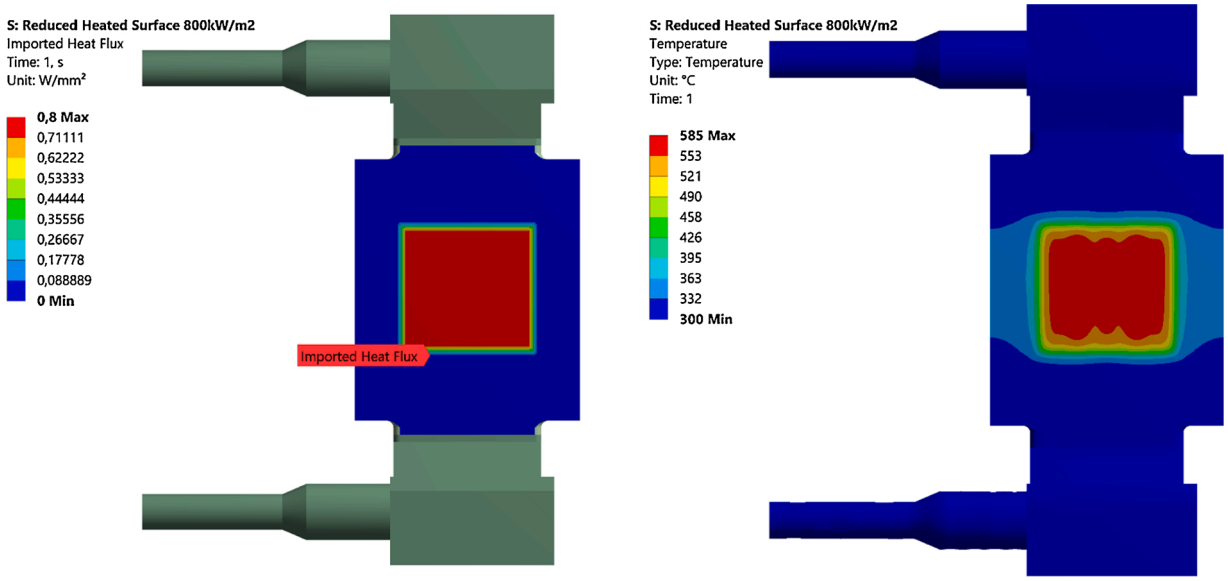

Fig. 16. Surface loading (left image) and simulated surface temperature distribution (right image) during the operation of the electron beam according to the reference scenario given in Table 4.

Table 5
The high heat flux fatigue test program for the mockup, performed in the HELOKA facility at KIT.

Test sequence	No. of cycles performed	Heat flux	Puls length (on/off)	Surface temperature
#1	100	0.7 MW/m^2	2 min/2 min	~550 °C
#2	100	0.8 MW/m^2	2 min/2 min	~600 °C
#3	100	0.9 MW/m^2	2 min/2 min	~650 °C
#4	7	0.9 MW/m^2	2 h / >2 min	~650 °C

switched on and off, each for a 2-minutes period for a predefined number of cycles.

Three fatigue test sequences with 100 cycles were conducted at surface temperatures of 550 °C, 600 °C, and 650 °C. Then a final sequence of 7 cycles with a pulse length of 2 h was performed. The test program is listed in Table 5.

During the first two test sequences in which the surface temperature of the mockup reached 550−600 °C, the operating parameters of the test facility indicated a stable performance. Therefore, we were confident enough to further increase the heat load in a third fatigue test sequence that raised the temperature to 650 °C. During this test sequence, all operating parameters remained within safe margins, indicating that the mockup did not start to crack or fail. The surface temperatures (maximum over time, transverse and longitudinal profiles) are plotted in Fig. 17, and Fig. 18 shows an infra-red photo of the mockup, taken during a heat load cycle in the 3rd test sequence.

The remaining operating time for testing our mockup was then used for a longer-pulse exposure at 650 °C surface temperatures. During the 7 pulses of 2 h each, creep or other thermal effects might be activated that would damage the mockup in a way. However, a peculiar change in the operating parameters did not appear. This indicated again that the structural integrity was most probably not affected.

In summary, the performed four test sequences of more than 300 high heat flux cycles in total can be marked as a full success. The predefined goals have not only been reached, but were even exceeded.

3.2. Microstructure analyses

After the high heat flux testing, we wanted to identify and investigate possible microstructural changes, defects, and surface modifications in the assumed critical zones of the mockup. For this, several cross-sections through the mockup were cut and prepared for optical and electron microscopy, i.e., Scanning Electron Microscopy (SEM) and Back Scattering Electron (BSE) imaging.

Prior to the microstructure analysis, a representative piece of the

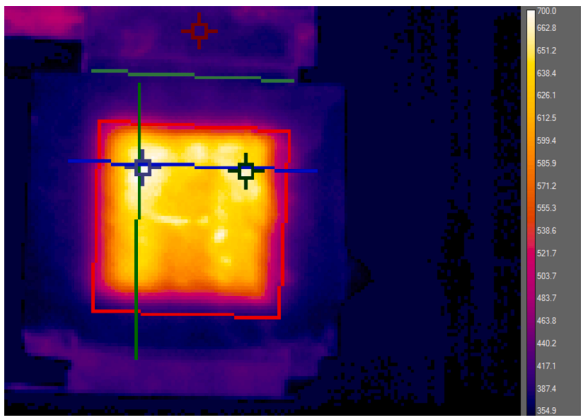

Fig. 18. Infra-red photo of the mockup during electron beam load of test sequence #3. The loaded area of 100 mm x 100 mm can be seen clearly. The perpendicular green line indicates the longitudinal and the horizontal blue line refers to the transvers profile in Fig. 17.

mock-up was selected and the mock-up was cut apart accordingly, which is illustrated in Fig. 19. From piece #3, a 10 mm thick section was cut and metallographically prepared by grinding and polishing for the SEM analysis.

In Fig. 20, back-scattering electrons (BSE) images of the ODS/EF97 interface were acquired close to channels A and C inside the high heat flux (HHF) loaded area. On the EUROFER97/2 side of the interface, an area of about 100 µm in width is recognizable that contains larger grains. In the following, we denote this area as heat affected zone (HAZ). In all images, the interface itself does not exhibit any defects, like Kirkendall voids, pores, cracks, delamination, or others.

To determine whether this HAZ has developed during the HHF test or earlier, during the diffusion bonding process, BSE images were acquired close to channel C in the hot area and close to the outer edge of the mockup in a cold area (see Fig. 21). As seen before, also here a clear HAZ is present in the hot interfacial region, whereas in the cold area no such feature appears in the BSE images. Nevertheless, there might still be a HAZ in the cold area, too, but it might be hidden due to the poorer polishing in this region. Therefore, we cannot draw a valid conclusion for the origin of the HAZ based on the BSE images.

Besides the structural changes that can be observed by imaging, chemical changes in the vicinity of the ODS/EUROFER interface are also of interest. For this, we acquired SEM-EDX elemental maps in and outside of the HHF loaded area. The result is shown in Fig. 22. Here, the C–K map shows in both areas no useful contrast, but only surface contamination. Both, the W-M and the Cr-K map show martensitic needle structure only in the lower part of the EUROFER97/2 region in both samples.

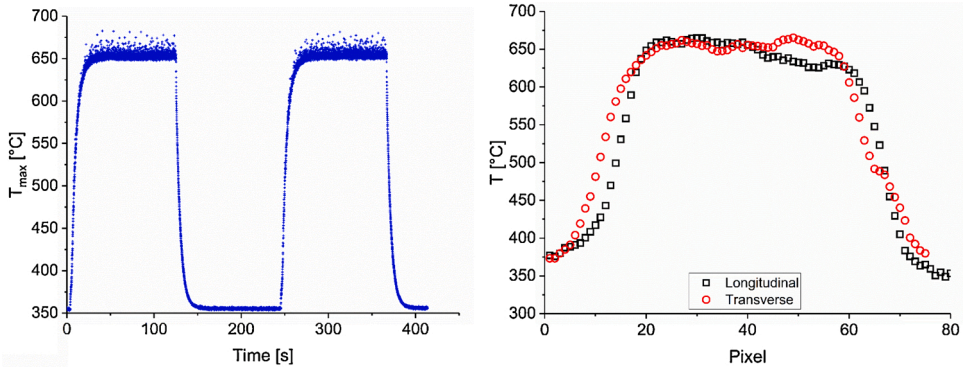

Fig. 17. (left) Test sequence #3: maximum surface temperature over time. (right) Surface temperature profile during electron beam load of test sequence #3 in longitudinal direction along the first channel (squares) and in transverse direction across all channels in about 50 mm distance from the outlet (circles). 50 pixels correspond approximately to 100 mm.

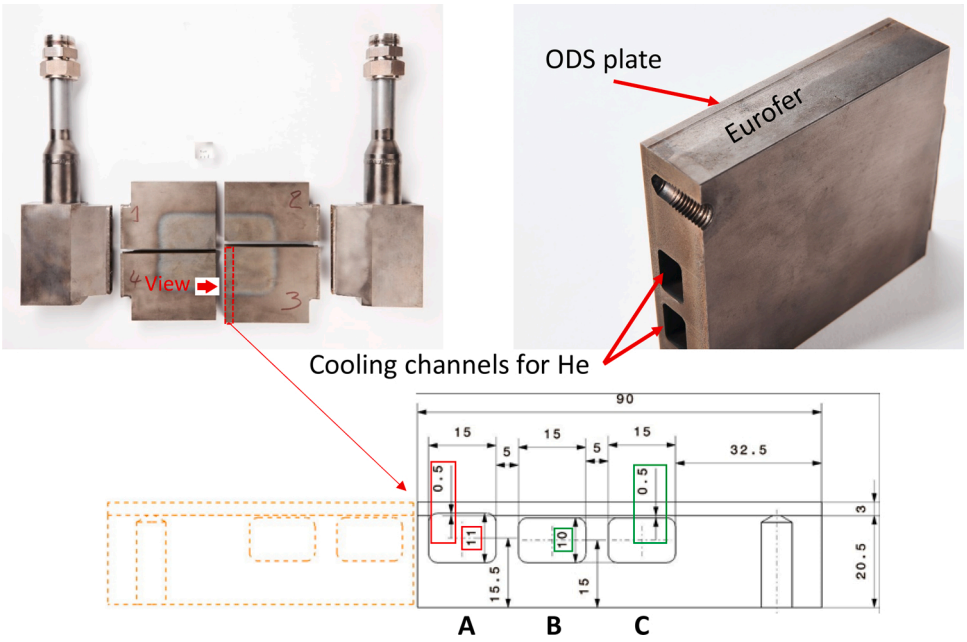

Fig. 19. Mockup pieces with labels 1-4 in top-down view (upper left). Sideview of piece #3 from which the SEM sample was cut (upper right). Technical drawing and identification of the cooling channel cross-sections A, B, C (lower part).

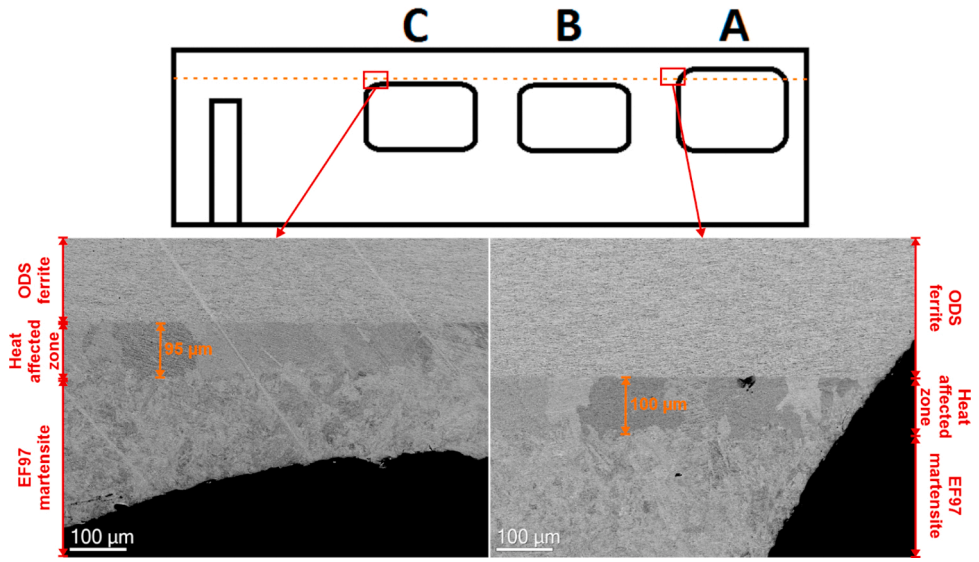

Fig. 20. Comparison of the BSE images acquired in the ODS/EF97 interfacial region close to channel C (left) and channel A (right).

But this means that there is indeed a HAZ – also in the cold area!

Further, this enables us to determine the width of the HAZs, which could not be done by analyzing the BSE image in the cold area. The width of the HAZ in the cold area (based on a measurement of the region without recognizable martensite laths or needles) amounts to about 55–60 µm, which is less than the 90–100 µm found in the HHF zone. Thus, we conclude that the formation mechanism of the HAZ has two stages: The first one is due to diffusion welding and the second one is due to HHF testing. Both processes provide conditions in which Cr and C diffusion can take place: during diffusion bonding the temperature is 1100 °C for 2 h and during the HHF test sequences 3 and 4 the interface is heated up to more that 500 °C for more than 15 h (according to a simulation of the area between the channels – in the interface directly over the channels, the temperature is even higher).

The width of the Cr diffusion zone (from the ODS ferrite into the EUROFER martensite) is comparable in both, the hot and the cold area. The density of Cr-rich precipitates in the ODS ferrite is increasing towards the interface. The Ti-K map shows Ti-rich precipitates in the ODS ferrite, likely at grain boundaries. The overall precipitation structure in the ODS ferrite is similar in both areas.

Furthermore, we could successfully determine the involved phases by performing a principal component analysis (PCA) on both SEM-EDX datasets. The results are presented in Fig. 23. In both areas, three phases (factors) were found: the Fe/Cr matrix, (Cr/W) carbides, and Ti carbonitrides. A noteworthy finding is that coarse Cr carbides precipitates are located in the ODS steel part of the interface. Their density increases towards the ODS/EUROFER interface. This is an indication for carbon diffusion from the EUROFER martensite into the ODS ferrite and might be noteworthy to be considered in future mockup or component fabrication. The second precipitate phase that was observed is Ti carbonitride and is only present in the ODS ferrite. Both precipitate phases are likely to be located at grain boundaries.

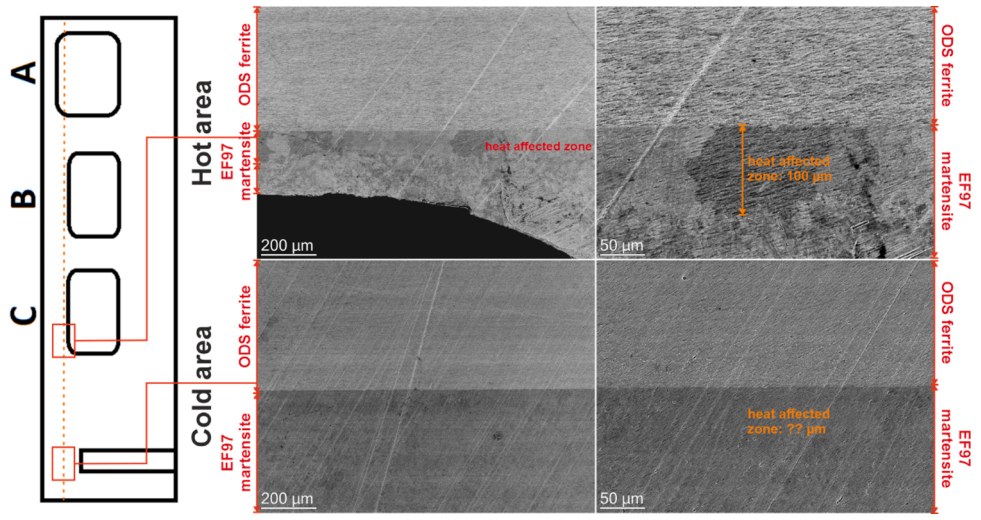

Fig. 21. Comparison of the BSE images acquired in ODS/EF97 interfacial area in the HHF (hot) area close to channel C and the cold outer region at different magnifications.

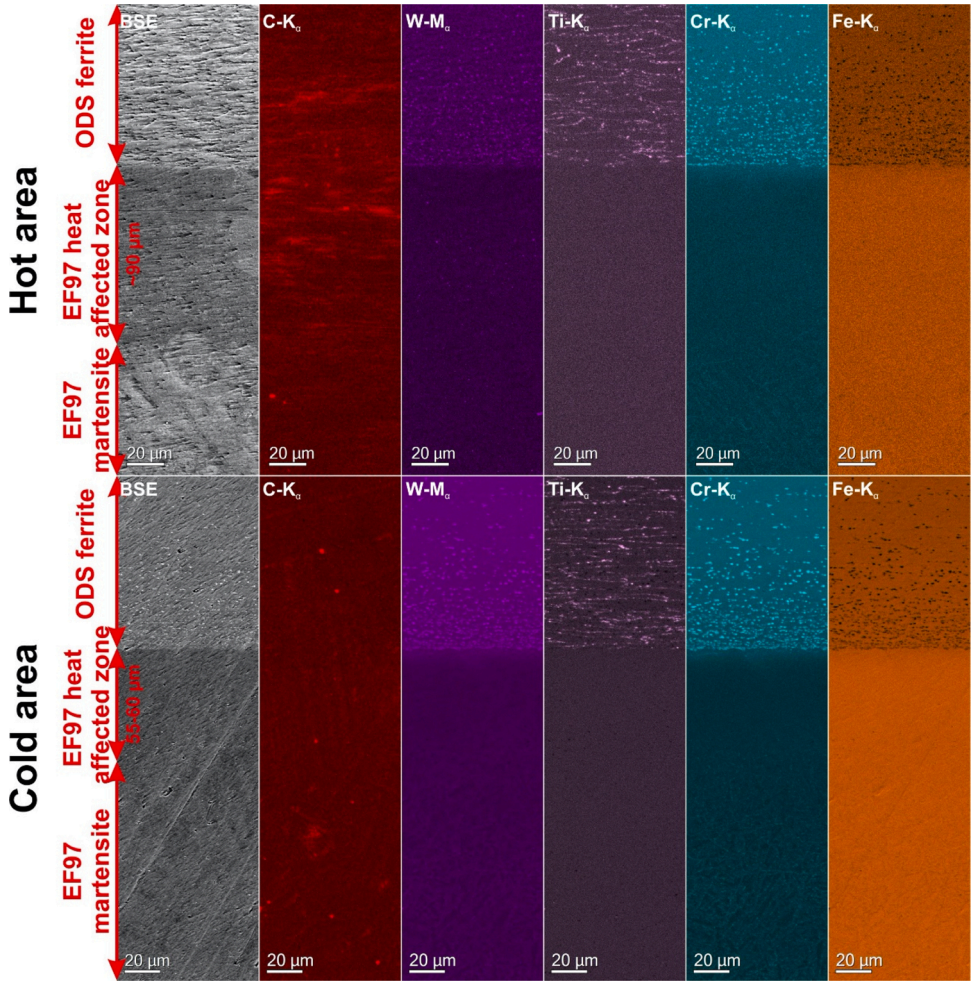

Fig. 22. SEM-EDX elemental mapping in the hot HHF region (upper part) and the cold outer region (lower part).

4. Summary and conclusions

For future power fusion power plants, but also for the blanket concepts of DEMO reactors, operating temperatures in the range of 450−550 °C (or higher) would be an effective measure to reduce irradiation hardening of the structural material (martensitic 9Cr steel – EUROFER97) significantly. In this case, the lifetime of breeding blankets (in particular helium-cooled components) would then be mainly determined by the thermo-mechanical load response (thermal fatigue) and by the accumulation and growth of helium bubbles (due to unavoidable

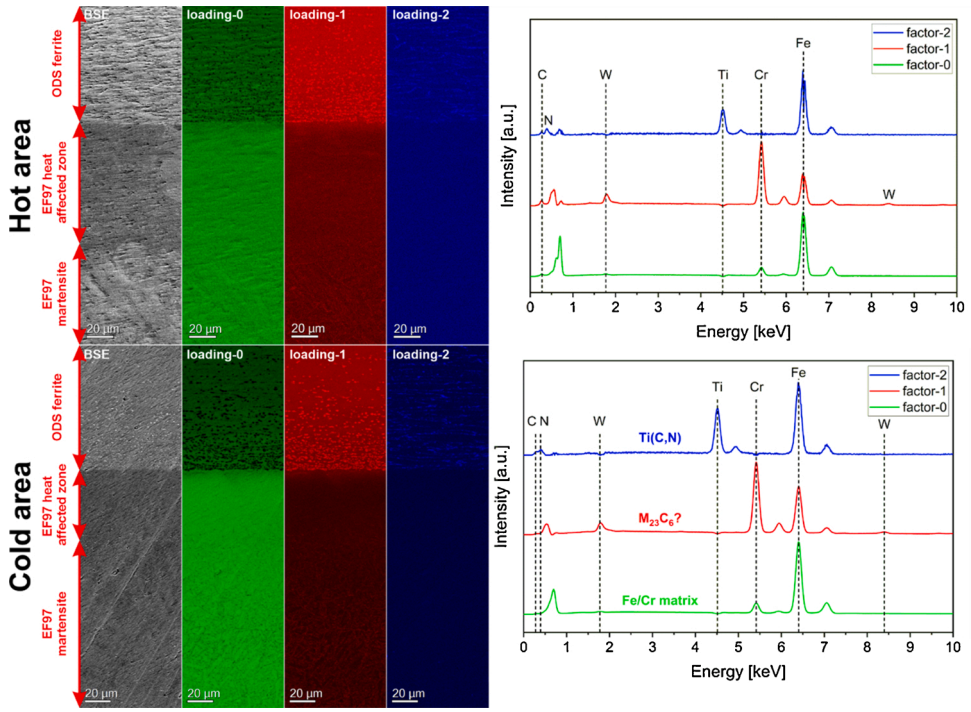

Fig. 23. Principal component analysis (PCA) of the SEM-EDX data presented in Fig. 22 to reveal the single phases, which are present in the respective sample area. The PCA generates two new datasets: one with the dimension of the signal space known as factors and the other with the dimension of the navigation space known as loadings.

transmutation). The presented strategy that could possibly overcome or at least mitigate the related design limits, consists of plating the plasma-facing surface of the blankets with thin ODS steel plates (a more effective strategy, but harder to realize, would be the replacement of the EUROFER by ODS steel within a layer of about 300 mm). Referring to the outline of the current project as presented in the introduction section, we want to highlight the following assessments and outcomes:

(1) With this project, we demonstrated the availability and maturity of industrial and commercially available fabrication, machining, and production processes, which are required for ODS steel plating of flat blanket first walls.
(2) By ODS steel plating, the surface operation temperature of a helium-cooled first wall mockup could be operated at 650 °C for 100 heat flux pulses of 2 min and for additional 7 cycles of 2 h each.
(3) The mockup could remove a heat flux of 0.9 MW/m^2 by helium cooling without flow promoters or other measures for an increased heat transfer.
(4) The mockup did not develop cracks or other tendencies to fail. Even at intentionally introduced weak points (i.e., the weld seams that were placed in one of the five cooling channels), crack formation did not occur.
(5) Further Post-experimental microstructural analyses by SEM did not reveal any critical changes (like Kirkendall pores, formation of brittle phases, aging, etc.) in and outside the interface region.
(6) The following microstructural features were recognized and analyzed:
   - Heat affected zone present in the EUROFER part below the interface
   - Two fractions of precipitates found inside the ODS plate: (i) Cr carbides and (ii) Ti(C,N)
   - Cr precipitate area density increases in the ODS steel towards the interface due to C diffusion from the EUROFER steel
   - Cr diffusion into EUROFER zone 5x smaller compared to heat affected zone

Declaration of Competing Interest

The authors declare that they have no conflict of interests.

Acknowledgments

We want to thank Daniel Bolich and Rainer Ziegler, both from Karlsruhe Institute of Technology (KIT, IAM), for their support regarding organization and dealing with infrastructural tasks like coordination of machining, photographing, and sample preparation. We are also grateful to the KIT CN workshop team with a special thanks to Tanja for the excellent EDM performance. Many thanks go to the group of chemical analysis headed by Thomas Bergfeld, KIT, IAM. Generally, we wish to express our gratitude to all colleagues who were involved the one or other way in this project.

This work has been carried out within the framework of the EUROfusion Consortium and has received funding from the Euratom research and training program 2014-2018 and 2019-2020 under grant agreement No 633053. The views and opinions expressed herein do not necessarily reflect those of the European Commission.

References

[1] G. Federici, W. Biel, M.R. Gilbert, R. Kemp, N. Taylor, R. Wenninger, European DEMO design strategy and consequences for materials, Nucl. Fusion 57 (2017), https://doi.org/10.1088/1741-4326/57/9/092002.
[2] G. Federici, C. Bachmann, L. Barucca, W. Biel, L. Boccaccini, R. Brown, C. Bustreo, S. Ciattaglia, F. Cismondi, M. Coleman, R. Wenninger, J.H. You, DEMO design activity in Europe: progress and updates, Fusion Eng. Des. 136 (2018) 729–741, https://doi.org/10.1016/j.fusengdes.2018.04.001.
[3] G. Federici, L. Boccaccini, F. Cismondi, M. Gasparotto, Y. Poitevin, I. Ricapito, An overview of the EU breeding blanket design strategy as an integral part of the DEMO design effort, Fusion Eng. Des. 141 (2019) 30–42, https://doi.org/10.1016/j.fusengdes.2019.01.141.
[4] G. Federici, C. Bachmann, L. Barucca, C. Baylard, W. Biel, L.V. Boccaccini, C. Bustreo, S. Ciattaglia, F. Cismondi, V. Corato, H. Walden, J.H. You, Overview of the DEMO staged design approach in Europe, Nucl. Fusion 59 (2019), https://doi.org/10.1088/1741-4326/ab1178.

[5] S. Baindur, Materials challenges for the supercritical water-cooled reactor (SCWR), Can. Nucl. Soc. - 28th Annu. Conf. Can. Nucl. Soc. 31st CNS/CNA Student Conf. 2007 "Embracing Futur. Canada'S Nucl. Renew. Growth." 2 (2007) 938–949.

[6] L. Santini, C. Accornero, A. Cioncolini, On the adoption of carbon dioxide thermodynamic cycles for nuclear power conversion: a case study applied to Mochovce 3 Nuclear Power Plant, Appl. Energy 181 (2016) 446–463, https://doi.org/10.1016/j.apenergy.2016.08.046.

[7] W. Zhou, Y. Yang, G. Zheng, K.B. Woller, P.W. Stahle, A.M. Minor, M.P. Short, Proton irradiation-decelerated intergranular corrosion of Ni-Cr alloys in molten salt, Nat. Commun. 11 (2020) 3430, https://doi.org/10.1038/s41467-020-17244-y.

[8] P.W. Humrickhouse, B.J. Merrill, S.-J. Yoon, L.C. Cadwallader, The impacts of liquid metal plasma-facing components on fusion reactor safety and tritium management, Fusion Sci. Technol. 75 (2019) 973–1001, https://doi.org/10.1080/15361055.2019.1658464.

[9] E. Gaganidze, J. Aktaa, Assessment of neutron irradiation effects on RAFM steels, Fusion Eng. Des. 88 (2013) 118–128, https://doi.org/10.1016/j.fusengdes.2012.11.020.

[10] M. Klimenkov, A. Möslang, E. Materna-Morris, H.-C. Schneider, Helium bubble morphology of boron alloyed EUROFER97 after neutron irradiation, J. Nucl. Mater. 442 (2013), https://doi.org/10.1016/j.jnucmat.2013.04.022.

[11] M. Klimenkov, A. Möslang, E. Materna-Morris, Helium influence on the microstructure and swelling of 9%Cr ferritic steel after neutron irradiation to 16.3 dpa, J. Nucl. Mater. 453 (2014) 54–59, https://doi.org/10.1016/j.jnucmat.2014.05.001.

[12] M. Klimenkov, E. Materna-Morris, A. Möslang, Boron effect on the microstructure of 9% Cr ferritic-martensitic steels, J. Nucl. Mater. 462 (2015) 280–288, https://doi.org/10.1016/j.jnucmat.2015.03.002.

[13] E. Materna-Morris, R. Lindau, H.-C. Schneider, A. Möslang, Tensile behavior of EUROFER ODS steel after neutron irradiation up to 16.3 dpa between 250 and 450 °c, Fusion Eng. Des. 98–99 (2015) 2038–2041, https://doi.org/10.1016/j.fusengdes.2015.07.015.

[14] M.R. Gilbert, S.L. Dudarev, S. Zheng, L.W. Packer, J.C. Sublet, An integrated model for materials in a fusion power plant: transmutation, gas production, and helium embrittlement under neutron irradiation, Nucl. Fusion 52 (2012), https://doi.org/10.1088/0029-5515/52/8/083019.

[15] F.A. Garner, in: R.J.M. Konings, R.E.B.T.-C.N.M (Eds.), 3.02 - Radiation-Induced Damage in Austenitic Structural Steels Used in Nuclear Reactors;, Elsevier, Oxford, 2020, pp. 57–168, https://doi.org/10.1016/B978-0-12-803581-8.12067-3 (Second E. Stoller (Eds.).

[16] M. Klimenkov, U. Jäntsch, M. Rieth, A. Möslang, Correlation of microstructural and mechanical properties of neutron irradiated EUROFER97 steel, J. Nucl. Mater. 538 (2020), https://doi.org/10.1016/j.jnucmat.2020.152231.

[17] A.V. Brabänder, J. Bredl, H.-C. Schneider, M. Kamlah, Registering hardness measurement of neutron-irradiated low-activation steels at high temperatures, Fusion Eng. Des. 146 (2019) 2734–2737, https://doi.org/10.1016/j.fusengdes.2019.05.008.

[18] C. Dethloff, E. Gaganidze, J. Aktaa, Review and critical assessment of dislocation loop analyses on EUROFER 97, Nucl. Mater. Energy 15 (2018) 23–26, https://doi.org/10.1016/j.nme.2018.05.015.

[19] H.-C. Schneider, C. Petersen, A.V. Povstyanko, A.E. Fedoseev, O. Makarov, Repeatability of irradiation damage and of recovery by post-irradiation annealing of EUROFER base steels, Fusion Eng. Des. 124 (2017) 1019–1023, https://doi.org/10.1016/j.fusengdes.2017.04.066.

[20] M. Klimenkov, R. Lindau, U. Jäntsch, A. Möslang, Effect of irradiation temperature on microstructure of ferritic-martensitic ODS steel, J. Nucl. Mater. 493 (2017) 426–435, https://doi.org/10.1016/j.jnucmat.2017.06.024.

[21] E. Materna-Morris, H.-C. Schneider, A. Möslang, Tensile behavior of RAFM alloys after neutron irradiation of up to 16.3 dpa between 250 and 450 °c, J. Nucl. Mater. 455 (2014) 728–734, https://doi.org/10.1016/j.jnucmat.2014.08.054.

[22] S. Sato, K. Maki, Analytical representation for neutron streaming through slits in fusion reactor blanket by Monte Carlo calculation, Fusion Eng. Des. 65 (2003) 501–524, https://doi.org/10.1016/S0920-3796(03)00003-6.

[23] S.J. Zinkle, L.L. Snead, Designing radiation resistance in materials for fusion energy, Annu. Rev. Mater. Res. 44 (2014) 241–267, https://doi.org/10.1146/annurev-matsci-070813-113627.

[24] P. He, M. Klimenkov, A. Möslang, R. Lindau, H.J. Seifert, Correlation of microstructure and low cycle fatigue properties for 13.5Cr1.1W0.3Ti ODS steel, J. Nucl. Mater. 455 (2014) 167–173, https://doi.org/10.1016/j.jnucmat.2014.05.024.

[25] I. Kubëna, J. Polák, P. Marmy, T. Kruml, A comparison of microstructure evolution due to fatigue loading in eurofer 97 and ODS eurofer steels, Procedia Eng. (2014) 401–404, https://doi.org/10.1016/j.proeng.2014.06.288.

[26] I. Kubëna, T. Kruml, J. Polák, Behaviour of ODS steels in cyclic loading, Trans. Indian Inst. Met. 69 (2016) 309–313, https://doi.org/10.1007/s12666-015-0814-3.

[27] L. Straßberger, A. Chauhan, S. Czink, J. Aktaa, High-temperature low-cycle fatigue behavior and microstructural evolution of an ODS steel based on conventional T91, Int. J. Fatigue 100 (2017) 50–57, https://doi.org/10.1016/j.ijfatigue.2017.03.012.

[28] A. Chauhan, L. Straßberger, U. Führer, D. Litvinov, J. Aktaa, Creep-fatigue interaction in a bimodal 12Cr-ODS steel, Int. J. Fatigue 102 (2017) 92–111, https://doi.org/10.1016/j.ijfatigue.2017.05.003.

[29] A. Chauhan, J. Hoffmann, D. Litvinov, J. Aktaa, High-temperature low-cycle fatigue behavior of a 9Cr-ODS steel: part 1 - pure fatigue, microstructure evolution and damage characteristics, Mater. Sci. Eng. A 707 (2017) 207–220, https://doi.org/10.1016/j.msea.2017.09.031.

[30] A. Chauhan, J. Hoffmann, D. Litvinov, J. Aktaa, High-temperature low-cycle fatigue behavior of a 9Cr-ODS steel: part 2 - hold time influence, microstructural evolution and damage characteristics, Mater. Sci. Eng. A 730 (2018) 197–206, https://doi.org/10.1016/j.msea.2018.05.107.

[31] L. Commin, M. Rieth, B. Dafferner, H. Zimmermann, D. Bolich, S. Baumgärtner, R. Ziegler, S. Dichiser, T. Fabry, S. Fischer, W. Hildebrand, O. Palussek, H. Ritz, A. Sponda, A fail-safe and cost effective fabrication route for blanket first walls, J. Nucl. Mater. 442 (2013), https://doi.org/10.1016/j.jnucmat.2013.07.043.

[32] D.T. Hoelzer, J. Bentley, M.K. Miller, M.K. Sokolov, T.S. Byun, M. Li, Development of nanostructured ferritic alloys discovery of nanostructured Ferritic alloys (NFA), Forum Am. Bar Assoc. (2010).

[33] S.J. Zinkle, J.L. Boutard, D.T. Hoelzer, A. Kimura, R. Lindau, G.R. Odette, M. Rieth, L. Tan, H. Tanigawa, Development of next generation tempered and ODS reduced activation ferritic/martensitic steels for fusion energy applications, Nucl. Fusion 57 (2017), 092005, https://doi.org/10.1088/1741-4326/57/9/092005.

[34] S. Ukai, M. Fujiwara, Perspective of ODS alloys application in nuclear environments, J. Nucl. Mater. 307–311 (2002) 749–757, https://doi.org/10.1016/S0022-3115(02)01043-7.

[35] B. Raj, M. Vijayalakshmi, Ferritic Steels and Advanced Ferritic-martensitic Steels, 2012, https://doi.org/10.1016/B978-0-08-056033-5.00066-5.

[36] F.A. Hernández, F. Arbeiter, L.V. Boccaccini, E. Bubelis, V.P. Chakin, I. Cristescu, B. E. Ghidersa, M. González, W. Hering, T. Hernández, X.Z. Jin, M. Kamlah, B. Kiss, R. Knitter, M.H.H. Kolb, P. Kurinskiy, O. Leys, I.A. Maione, M. Moscardini, G. Nádasi, H. Neuberger, P. Pereslavtsev, S. Pupeschi, R. Rolli, S. Ruck, G. A. Spagnuolo, P.V. Vladimirov, C. Zeile, G. Zhou, Overview of the HCPB research activities in EUROfusion, IEEE Trans. Plasma Sci. 46 (2018) 2247–2261, https://doi.org/10.1109/TPS.2018.2830813.

[37] F.A. Hernández, P. Pereslavtsev, G. Zhou, H. Neuberger, J. Rey, Q. Kang, L. V. Boccaccini, E. Bubelis, I. Moscato, D. Dongiovanni, An enhanced, near-term HCPB design as driver blanket for the EU DEMO, Fusion Eng. Des. (2019), https://doi.org/10.1016/j.fusengdes.2019.02.037.

[38] F.A. Hernández, P. Pereslavtsev, G. Zhou, B. Kiss, Q. Kang, H. Neuberger, V. Chakin, R. Gaisin, P. Vladimirov, L.V. Boccaccini, G.A. Spagnuolo, S. D'Amico, I. Moscato, Advancements in the helium-cooled pebble bed breeding blanket for the EU DEMO: holistic design approach and lessons learned, Fusion Sci. Technol. 75 (2019) 352–364, https://doi.org/10.1080/15361055.2019.1607695.

[39] H. Neuberger, J. Rey, A. Von Der Weth, F. Hernandez, T. Martin, M. Zmitko, A. Felde, R. Niewöhner, F. Krüger, Overview on ITER and DEMO blanket fabrication activities of the KIT INR and related frameworks, Fusion Eng. Des. 96–97 (2015) 315–318, https://doi.org/10.1016/j.fusengdes.2015.06.174.

[40] H. Neuberger, J. Rey, F. Arbeiter, F. Hernandez, S. Ruck, C. Koehly, L. Stratil, R. Niewöhner, A. Felde, Evaluation of conservative and innovative manufacturing routes for gas cooled test blanket module and breeding blanket first walls, Fusion Eng. Des. 146 (2019) 2140–2143, https://doi.org/10.1016/j.fusengdes.2019.03.124.

[41] M. Rieth, J. Rey, Specific welds for test blanket modules, J. Nucl. Mater. 386–388 (2009) 471–474, https://doi.org/10.1016/j.jnucmat.2008.12.142.

[42] M. Rieth, B. Dafferner, S. Baumgärtner, S. Dichiser, T. Fabry, S. Fischer, W. Hildebrand, O. Palussek, H. Ritz, A. Sponda, R. Ziegler, H. Zimmermann, Cost Effective Fabrication of a Fail-Safe First Wall, 2010. http://bibliothek.fzk.de/zb/veroeff/81118.htm.

[43] B.E. Ghidersa, M. Ionescu-Bujor, G. Janeschitz, Helium Loop Karlsruhe (HELOKA): a valuable tool for testing and qualifying ITER components and their He cooling circuits, Fusion Eng. Des. 81 (2006) 1471–1476, https://doi.org/10.1016/J.FUSENGDES.2005.06.370.

[44] B.E. Ghidersa, V. Marchese, M. Ionescu-Bujor, T.H. Ihli, HELOKA facility: thermo-hydrodynamic model and control, Fusion Eng. Des. 83 (2008) 1792–1796, https://doi.org/10.1016/j.fusengdes.2008.06.016.

[45] B.E. Ghidersa, X. Jin, M. Rieth, M. Ionescu-Bujor, KATHELO: a new high heat flux component testing facility, Fusion Eng. Des. 88 (2013), https://doi.org/10.1016/j.fusengdes.2013.02.065.

[46] S. Ranjithkumar, B.K. Yadav, A. Saraswat, P. Chaudhuri, E.R. Kumar, A. Kunze, B. E. Ghidersa, Performance assessment of the Helium cooled First Wall mock-up in HELOKA facility, Fusion Eng. Des. 150 (2020), 111319, https://doi.org/10.1016/j.fusengdes.2019.111319.

[47] KTA 3102.1 - reactor core design for High-temperature gas-cooled reactors part 1: calculation of the material properties of helium, Geschäftsstelle des Kerntechnischen Ausschusses beim Bundesamt für Strahlenschutz, 38259 Salzgitter, Germany, 1978.